PLOS ONE

RESEARCH ARTICLE

Research on the deformation law for flat rolling of a core filled tube based on the slab method

Junlong Qi[1], **Xianghua Liu**[1,2]*, **Haitao Gao**[1], **Xiangkun Sun**[1]

1 State Key Laboratory of Rolling and Automation, Northeastern University, Shenyang, China, **2** Key Laboratory of Lightweight Structural Materials, Liaoning Province, Shenyang, China

* liuxh@mail.neu.edu.cn

Abstract

The deformation law for axisymmetric deformation during the drawing of a core filled tube (CORFT) has been studied. However, the results of such studies could not be used in the flat rolling process of the CORFT, which is a plan deformation condition. In this paper, the inner core material and outer steel tube were successively analyzed based on the slab method during the flat rolling process (plan deformation) of the CORFT, and equations for wall thickness, core density, and roll force have been developed. The theoretical results solved by the developed equations were compared with the experimental results, revealing adequate accuracy for engineering requirements. The influences of rolling parameters on the roll force and the ultimate value of the relative density of the core material were studied, and the limiting condition for a larger roll force or higher value for relative density was obtained.

Citation: Qi J, Liu X, Gao H, Sun X (2020) Research on the deformation law for flat rolling of a core filled tube based on the slab method. PLoS ONE 15(8): e0237039. https://doi.org/10.1371/journal.pone.0237039

Editor: Guangyong Sun, Hunan University, CHINA

Received: June 17, 2020

Accepted: July 17, 2020

Published: August 10, 2020

Data Availability Statement: All relevant data are within the paper.

Funding: The authors received no specific funding for this work.

Competing interests: The authors have declared that no competing interests exist.

1 Introduction

Energy-saving [1] is an important factor for the iron and steel industry. A core filled tube (CORFT) [2] is prepared using blast furnace slag (BFS), which is typical solid waste in the iron and steel industry that has broad economic and environmental benefits. A CORFT prepared using the technology proposed in the literatures [2, 3] is shown in Fig 1(A). The CORFT is composed of Q235 steel tube and granular BFS, and it can be used as a substitute for flat steel in fences, and stair railings, as shown in (Fig 1B and 1C).

Studies of the rolling process of powder/solid composite clad rods, such as high-temperature superconducting (HTS) [4–7] and sheath materials [8, 9] have been conducted. Han et al. [10] studied the deformation law of Bi-HTS materials during the rolling process and found the critical density (the ultimate value of the powder) of the inner superconducting powder. They found that the critical density was influenced by the size and shape of the inner granule, the yield strength of the outer steel tube, and the key parameter of the ratio between the thickness and length of the deformation zone h/l but remained unchanged with different packing densities of the core material. Korzekwa et al. [11] studied the influence of process parameters on spread during the rolling of HTS materials. The parameters of concern included roll diameter,

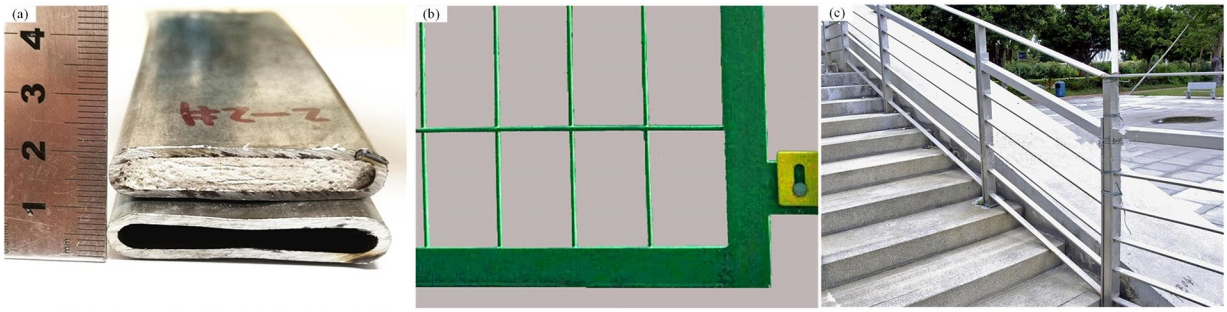

Fig 1. Products in which CORFTs are used. (a) Core filled tube and tube, (b) fences, and (c) stair railings.

https://doi.org/10.1371/journal.pone.0237039.g001

packing density, reduction rate, and the initial width of the HTS material. Pandheeradi et al. [12] adopted the finite element method to simulate the rolling process of HTS materials. Then, experiments were conducted to verify the accuracy of the simulation. Lu et al. [13] simulated the influences of initial shape on the homogeneity and density of the core material of a HTS system during the rolling process and verified the simulation by conducting experiments. Lu [14] studied the cause and influencing factors of the sausage effect (the thickness of the powder changes along with the coordinate in the length direction) for multiple HTS tapes. The rolling process was simulated using the finite element method, and the influences of roll diameter, coefficient of friction, and yield strength on the sausage effect were analyzed. Jiang et al. [15] simulated the cold rolling of a thin strip with different friction models using a three-dimensional rigid-plastic finite element method. The roll separating force, spread and forward slip for constant friction and friction variation models were compared. The friction variation in the roll bite has a significant effect on the simulation results. Cavaliere et al. [16] built a finite element model to analyze the hot rolling of steel coils and the hot mandrel rolling of a seamless steel tube.

In a previous report [17], a slab method was adopted to analyze the drawing process of the CORFT, which was an axisymmetric deformation problem. However, the previous rules cannot be used during the flat rolling process of the CORFT, which is a plan deformation problem. In this paper, first the inner core material and outer steel tube were successively analyzed based on the slab method [18–21] during the flat rolling process (plan deformation) of the CORFT, and equations for wall thickness s, the relative density z of the core material (the ratio between the core density and the granular density of the core material), and roll force F_d were developed. Then, flat rolling experiments on tubes and CORFTs were conducted, and the theoretical results solved by the developed equations were compared with the experimental results. Finally, using the theoretical equations, the influences of the rolling parameters on the roll force F_d and the ultimate value of the relative density z_U of the core material were calculated and analyzed.

2 Theoretical research on the flat rolling of a core filled tube

2.1 Parameters of the deformation zone

The basic parameters of the CORFT during the flat rolling process are shown in Fig 2. Fig 2(A) is the cross section of the preformed billet. Because of the low deformation, the thickness of the outer steel tube remained unchanged and the value was s_0 during the pre-rolling process of the CORFT. The thickness, total width and the contact width between the rolled billet and the roll for the preformed billets are denoted as H_0, B_0 and B_{c0}. As shown in (Fig 2B and 2C), the outer and inner layer of the CORFT are a steel tube and BFS, respectively. The thickness of the

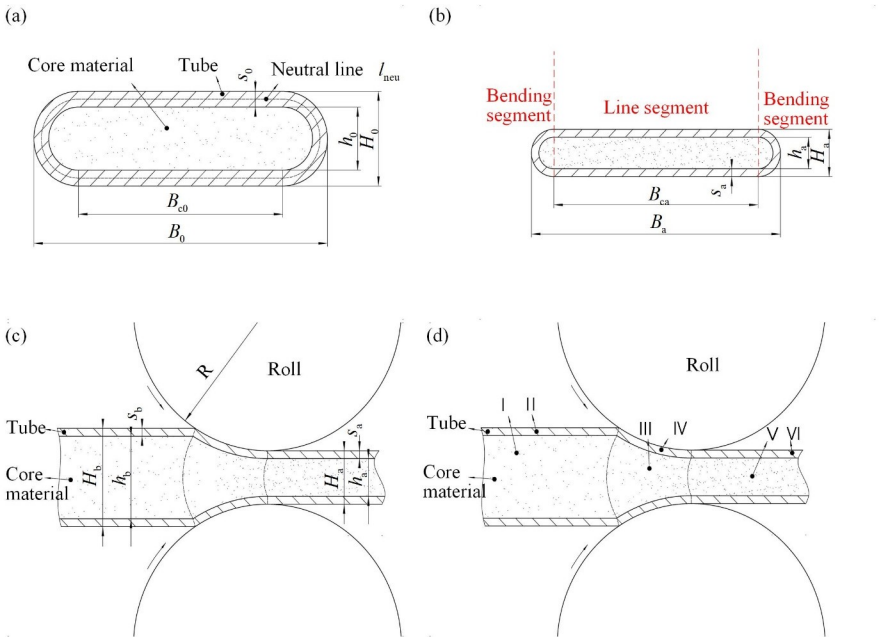

Fig 2. Section of the flat rolling process. (a) Cross section of preformed billet, (b) cross section at the outlet side, (c) vertical section, and (d) division of the deformation zone.

https://doi.org/10.1371/journal.pone.0237039.g002

core material, the outer steel tube, and the total rolled billet before the flat rolling process are h_b, s_b and H_b, respectively, and they change into h_a, s_a and H_a, respectively, after the flat rolling process. The roll radius is R and the total width of the rolled billet and the contact width between the rolled billet and the roll are B_b and B_{cb} before the rolling process and become B_a and B_{ca} after the rolling process. The steel tube can be divided into a line segment and a bending segment, as shown in Fig 2(B). During the flat rolling process of the CORFT, the deformation zone is divided into six areas I to VI, as shown in Fig 2(D). Among the six areas, areas III and IV are deformation areas, and the other areas are the outer areas.

2.2 Analysis of the two stages

The flat rolling process of the CORFT can be divided into two steps: the compressive stage and the elongation stage. During the compressive stage, the holding power on the inner surface of the steel tube, which is provided by the inner core material, is not sufficient. Thus, only the outer steel tube bends; the wall thickness and the length of the steel tube remain unchanged. When the thickness of the rolled billet becomes less than the critical thickness H_c, the flat rolling process transforms into the elongation stage. During this stage, the holding power is sufficient, thus the wall thickness starts to decrease, and the length of the steel tube begins to extend.

During the compressive stage, both the wall thickness and the length of the steel tube remain unchanged, or:

$$\begin{cases} s_a = s_0 \\ l_{ta} = l_{t0} \end{cases} \tag{1}$$

During the elongation stage, neglecting the slide spread of the rolled billet, the volumetric stain (ε_{Vb} and ε_{Va}) of the core material before and after the flat rolling process can be denoted

as:

$$\begin{cases} -\varepsilon_{\mathrm{Vb}} = \ln \dfrac{h_0}{h_{\mathrm{b}} \cdot \lambda_0} \\ -\varepsilon_{\mathrm{Va}} = \ln \dfrac{h_0}{h_{\mathrm{a}} \cdot \lambda_0 \cdot \lambda} = -\varepsilon_{\mathrm{Vb}} + \ln \dfrac{h_{\mathrm{b}}}{h_{\mathrm{a}} \cdot \lambda} \end{cases} \tag{2}$$

where $\varepsilon_{\mathrm{Vb}}$ and $\varepsilon_{\mathrm{Va}}$ are the volumetric strains of the core material before and after the flat rolling process, respectively, h_{b} and h_{a} are the thicknesses of the core material before and after the flat rolling process, λ_0 is the total accumulated elongation coefficient of the core material before the rolling pass, and λ is the elongation coefficient of the core material during the flat rolling pass.

Experiments in a previous study [17] showed that the relationship between the compressive stress p_{y} and the volumetric strain ε_{V} obeyed an exponential model, and it could be described as

$$p_{\mathrm{y}} = \mathrm{A}_1 \cdot \exp\left(\frac{-\varepsilon_{\mathrm{V}}}{\mathrm{A}_2}\right) \tag{3}$$

where A_1 and A_2 are two constants that could be fitted from the experimental data with values of 0.390 and 0.0816, respectively.

Substituting Eq (2) into (3), the compressive stress (p_{yb} and p_{ya}) of the core material before and after the flat rolling process can be denoted as:

$$\begin{cases} p_{\mathrm{yb}} = \mathrm{A}_1 \cdot \exp\left(\dfrac{-\varepsilon_{\mathrm{Vb}}}{\mathrm{A}_2}\right) = \mathrm{A}_1 \left(\dfrac{h_0}{h_{\mathrm{b}} \cdot \lambda_0}\right)^{\dfrac{1}{\mathrm{A}_2}} \\ p_{\mathrm{ya}} = p_{\mathrm{yb}} \cdot \exp\left(\dfrac{-\varepsilon_{\mathrm{Va}} + \varepsilon_{\mathrm{Vb}}}{\mathrm{A}_2}\right) = p_{\mathrm{yb}} \cdot \left[\dfrac{(H_{\mathrm{b}} - 2s_{\mathrm{b}}) \cdot s_{\mathrm{a}}}{(H_{\mathrm{a}} - 2s_{\mathrm{a}}) \cdot s_{\mathrm{b}}}\right]^{\dfrac{1}{\mathrm{A}_2}} \end{cases} \tag{4}$$

2.3 Stress analysis of the inner core material

The CORFT consists of the inner core material and the outer steel tube. Thus, the force condition of the inner core material and the outer steel tube should be analyzed successively to analyze the force condition for the flat rolling process of the CORFT. To analyze the stress state of the core material, the following assumptions should be made:

1. The influence of the core material in the bending segment during the flat rolling process of the CORFT is neglected.
2. The slide spread of the outer steel tube is neglected, and the flat rolling process of the CORFT is regarded as plain deformation.
3. The coulomb friction law is used for the contact surfaces.
4. The normal stress σ_{ix} on a surface of the core material slab is distributed uniformly.
5. When the hydrostatic pressure p of the core material reaches a certain value p_{y}, the volume of the core material shrinks, or the porosity of the core material decreases. Then,

$$\frac{\sigma_{\mathrm{ix}} + p_{\mathrm{ix}}}{2} = p_{\mathrm{y}} \tag{5}$$

Or,

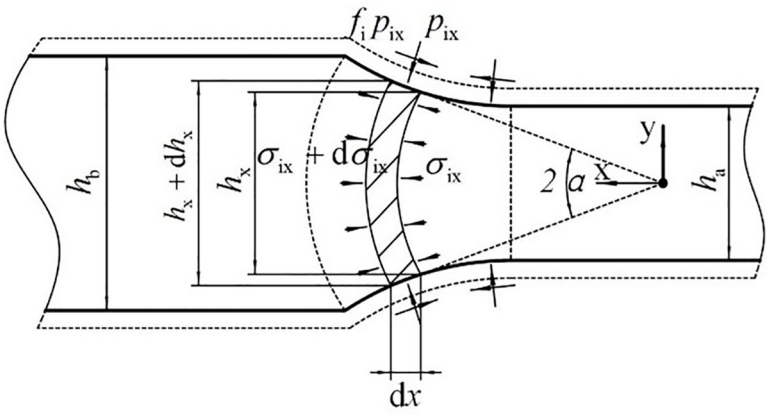

Fig 3. Stress analysis of the microunit of the core material.

https://doi.org/10.1371/journal.pone.0237039.g003

$$\sigma_{ix} = 2p_y - p_{ix} \tag{6}$$

where σ_{ix} and p_{ix} are the pressures of the core material in the x direction and are perpendicular to the contact surface between the steel tube and the core material, respectively, MPa.

Stress analysis is done on the microunit of the deformation zone for the core material, as shown in Fig 3.

According to the static equilibrium of the core material in the x direction, it can be deduced that:

$$(\sigma_{ix} + d\sigma_{ix})(h_x + dh_x) - \sigma_{ix}h_x - 2p_{ix} \cdot \frac{dx}{\cos\alpha} \cdot \sin\alpha \mp 2f_i p_{ix} dx = 0 \tag{7}$$

where—and + in $\mp$ denote the forward and backward slide zones, respectively.

Eq (6) can be transformed into:

$$dp_{ix} = -d\sigma_{ix} \tag{8}$$

Eqs (6), (8) and $\tan\alpha = dh_x/(2dx)$ are substituted into (7), and then,

$$\frac{dp_{ix}}{dx} + \frac{2(p_{ix} - p_y)}{h_x} \cdot \frac{dh_x}{dx} \pm \frac{2f_i p_{ix}}{hA_x} = 0 \tag{9}$$

With a small bite angle, the contact arc can be substituted with a chord, or,

$$h_x = \frac{h_b - h_a}{l} x + h_a \tag{10}$$

Or,

$$dx = \frac{l}{\Delta h} dh_x \tag{11}$$

The above equation is substituted into (9), and then,

$$\frac{\mathrm{d}p_{\mathrm{ix}}}{\left(-2\mp\frac{2f_{\mathrm{i}}l}{\Delta h}\right)p_{\mathrm{ix}}+2p_{\mathrm{y}}}=\frac{\mathrm{d}h_{\mathrm{x}}}{h_{\mathrm{x}}} \tag{12}$$

After integration, the equation can be denoted as follows:

$$p_{\mathrm{ix}}=\mathrm{C_i}h_{\mathrm{x}}{}^{-2\mp\frac{2f_{\mathrm{i}}l}{\Delta h}}+\frac{2p_{\mathrm{y}}}{2\pm\frac{2f_{\mathrm{i}}l}{\Delta h}} \tag{13}$$

At the forward slide zone, when $h_{\mathrm{x}}=h_{\mathrm{a}}$, the equation can be denoted as follows:

$$p_{\mathrm{ix}}=2p_{\mathrm{y}}-\sigma_{\mathrm{ixa}} \tag{14}$$

where σ_{ixa} is the stress of the core material in the x direction at zone V, MPa.

Eq (14) is substituted into (13) while letting $\xi_{\mathrm{i1}}=1\text{-}\sigma_{\mathrm{ixa}}/(2p_{\mathrm{ya}})$ and $\delta_{\mathrm{i1}}=2f_{\mathrm{i}}l/\Delta h+2$, then,

$$p_{\mathrm{ix}}=\frac{2p_{\mathrm{y}}}{\delta_{\mathrm{i1}}}\left[(\xi_{\mathrm{i1}}\delta_{\mathrm{i1}}-1)\left(\frac{h_{\mathrm{a}}}{h_{\mathrm{x}}}\right)^{\delta_{\mathrm{i1}}}+1\right] \tag{15}$$

In the backward slide zone, when $h_{\mathrm{x}}=h_{\mathrm{b}}$, the equation can be denoted as follows:

$$p_{\mathrm{ix}}=2p_{\mathrm{y}}-\sigma_{\mathrm{ixb}} \tag{16}$$

where σ_{ixb} is the stress of the core material in the x direction at zone I, MPa.

Eq (16) is substituted into (13) while letting $\xi_{\mathrm{i2}}=1\text{-}\sigma_{\mathrm{ixb}}/(2p_{\mathrm{yb}})$ and $\delta_{\mathrm{i2}}=2f_{\mathrm{i}}l/\Delta h\text{-}2$, then,

$$p_{\mathrm{ix}}=\frac{2p_{\mathrm{y}}}{\delta_{\mathrm{i2}}}\left[(\xi_{\mathrm{i2}}\delta_{\mathrm{i2}}+1)\left(\frac{h_{\mathrm{x}}}{h_{\mathrm{b}}}\right)^{\delta_{\mathrm{i2}}}-1\right] \tag{17}$$

At the demarcation plane between the forward and backward slide zones, or the neutral plane, substituting $h_{\mathrm{x}}=h_{\gamma}$ into Eqs (15) and (17) can be denoted as follows:

$$\delta_{\mathrm{i1}}(\xi_{\mathrm{i2}}\delta_{\mathrm{i2}}+1)h_{\gamma}{}^{\delta_{\mathrm{i1}}+\delta_{\mathrm{i2}}}-(\delta_{\mathrm{i1}}+\delta_{\mathrm{i2}})h_{\mathrm{b}}{}^{\delta_{\mathrm{i2}}}\cdot h_{\gamma}{}^{\delta_{\mathrm{i1}}}-\delta_{\mathrm{i2}}(\xi_{\mathrm{i1}}\delta_{\mathrm{i1}}-1)h_{\mathrm{b}}{}^{\delta_{\mathrm{i2}}}\cdot h_{\mathrm{a}}{}^{\delta_{\mathrm{i1}}}=0 \tag{18}$$

where h_{γ} is thickness of the core material at the neutral plan, mm and $h_{\mathrm{a}}\leq h_{\gamma}\leq h_{\mathrm{b}}$.

h_{γ} can be determined by using a dichotomy. By integrate the parameter p_{ix} over the whole deformation zone, the compressive force P_{i} of the core material can be obtained as follows:

$$\begin{aligned}\mathrm{P_i}=&\frac{2\mathrm{p_y}\cdot(\mathrm{B_{cb}}+\mathrm{B_{ca}})}{2}\\&\times\left\{\frac{1}{\delta_{\mathrm{i1}}}\int_0^{\mathrm{x}_{\gamma}}\left[(\xi_{\mathrm{i1}}\delta_{\mathrm{i1}}-1)\left(\frac{\mathrm{h_a}}{\mathrm{h_x}}\right)^{\delta_{\mathrm{i1}}}+1\right]\mathrm{dx}+\frac{1}{\delta_{\mathrm{i2}}}\int_{\mathrm{x}_{\gamma}}^{1}\left[(\xi_{\mathrm{i2}}\delta_{\mathrm{i2}}+1)\left(\frac{\mathrm{h_x}}{\mathrm{h_b}}\right)^{\delta_{\mathrm{i2}}}-1\right]\mathrm{dx}\right\}\end{aligned} \tag{19}$$

where B_{cb} and B_{ca} are the contact widths between the CORFT and the roll for the inlet and outlet side, mm, and P_{i} is the compressive force of the core material, MPa.

Substituting Eq (11) into the above equation can be denoted as follows:

$$P_{\mathrm{i}}=\frac{2p_{\mathrm{y}}\cdot(B_{\mathrm{cb}}+B_{\mathrm{ca}})}{2}\times\frac{l}{\Delta h}\left\{-\frac{(\xi_{\mathrm{i1}}\delta_{\mathrm{i1}}-1)\cdot h_{\gamma}}{\delta_{\mathrm{i1}}(\delta_{\mathrm{i1}}-1)}\left(\frac{h_{\mathrm{a}}}{h_{\gamma}}\right)^{\delta_{\mathrm{i1}}}-\frac{(\xi_{\mathrm{i2}}\delta_{\mathrm{i2}}+1)\cdot h_{\gamma}}{\delta_{\mathrm{i2}}(\delta_{\mathrm{i2}}+1)}\left(\frac{h_{\gamma}}{h_{\mathrm{b}}}\right)^{\delta_{\mathrm{i2}}}+\frac{\xi_{\mathrm{i1}}-1}{\delta_{\mathrm{i1}}-1}\cdot h_{\mathrm{a}}+\frac{\xi_{\mathrm{i2}}-1}{\delta_{\mathrm{i2}}+1}\cdot h_{\mathrm{b}}+h_{\gamma}\right\}\quad(20)$$

Then, the average compressive stress $\bar{p}_{\mathrm{i}}$ can be solved as follows:

$$\bar{p}_{\mathrm{i}}=\frac{2p_{\mathrm{y}}}{\Delta h}\left\{-\frac{(\xi_{\mathrm{i1}}\delta_{\mathrm{i1}}-1)\cdot h_{\gamma}}{\delta_{\mathrm{i1}}(\delta_{\mathrm{i1}}-1)}\left(\frac{h_{\mathrm{a}}}{h_{\gamma}}\right)^{\delta_{\mathrm{i1}}}-\frac{(\xi_{\mathrm{i2}}\delta_{\mathrm{i2}}+1)\cdot h_{\gamma}}{\delta_{\mathrm{i2}}(\delta_{\mathrm{i2}}+1)}\left(\frac{h_{\gamma}}{h_{\mathrm{b}}}\right)^{\delta_{\mathrm{i2}}}+\frac{\xi_{\mathrm{i1}}-1}{\delta_{\mathrm{i1}}-1}\cdot h_{\mathrm{a}}+\frac{\xi_{\mathrm{i2}}-1}{\delta_{\mathrm{i2}}+1}\cdot h_{\mathrm{b}}+\left(\frac{1}{\delta_{\mathrm{i1}}}+\frac{1}{\delta_{\mathrm{i2}}}\right)\cdot h_{\gamma}\right\}\quad(21)$$

where $\bar{p}_{\mathrm{i}}$ is the average compressive stress, MPa.

2.4 Stress analysis for the outer steel tube

Based on the average compressive stress $\bar{p}_{\mathrm{i}}$ of the core material, the stress state of the outer steel tube should be studied to analyze the stress state of the flat rolling process of the CORFT. To analyze the stress state of the outer steel tube, the following assumptions should be made:

1. The influence of the bending segment during the flat rolling process of the CORFT is neglected, and just the line segment is considered.
2. The slide spread of the outer steel tube is neglected, and the flat rolling process of the CORFT is regarded as plain deformation.
3. The coulomb friction law is used for the contact surfaces.
4. The normal stress σ_{x} on a same surface of the steel tube slab is distributed uniformly.
5. The approximate yield criterion of the outer steel tube can be denoted as:

$$p_{\mathrm{x}}-\sigma_{\mathrm{x}}=K\quad(22)$$

where σ_{x} and p_{x} are pressures of the steel tube in the x direction and perpendicular to the contact surface between the roll and the steel tube, MPa.

As shown in Fig 4, according to the static equilibrium of the outer steel tube in the y direction ($\sum Y=0$), it can be denoted as follows:

$$(p_{\mathrm{ix}}-p_{\mathrm{x}})\cdot\frac{\mathrm{d}x}{\cos\alpha}\cdot\cos\alpha\pm(fp_{\mathrm{x}}-f_{\mathrm{i}}p_{\mathrm{ix}})\cdot\frac{\mathrm{d}x}{\cos\alpha}\cdot\sin\alpha=0\quad(23)$$

Simplifying the above equation gives

$$p_{\mathrm{ix}}=\frac{1\mp f\tan\alpha}{1\mp f_{\mathrm{i}}\tan\alpha}\cdot p_{\mathrm{x}}\quad(24)$$

The $f\tan\alpha$ and $f_{\mathrm{i}}\tan\alpha$ are parameters far less than 1, so the equation can be denoted as follows:

$$p_{\mathrm{ix}}\approx p_{\mathrm{x}}\quad(25)$$

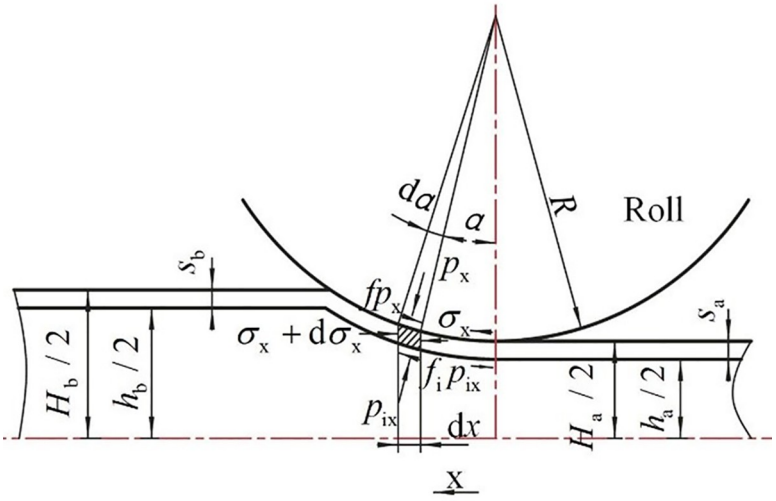

Fig 4. Stress analysis for the microunit of the steel tube.

https://doi.org/10.1371/journal.pone.0237039.g004

Based on Eq (25), according to the static equilibrium of the outer steel tube in the x direction the equation can be denoted as follows:

$$(\sigma_x + d\sigma_x)(s_x + ds_x) - \sigma_x s_x \mp (f - f_i) p_x \cdot \frac{dx}{\cos\alpha} \cdot \cos\alpha = 0 \tag{26}$$

where–and + in $\mp$ denote the forward and backward slide zones, respectively.

It can be deduced from Eq (22) that,

$$dp_x = d\sigma_x \tag{27}$$

Substituting Eqs (22) and (27) into (26) gives

$$\frac{dp_x}{dx} + \frac{p_x - K}{s_x} \times \frac{ds_x}{dx} \mp \frac{f - f_i}{s_x} p_x = 0 \tag{28}$$

Considering that the variation of parameter s_x is small, s_x can be assumed to change linearly in the x direction:

$$s_x = \frac{s_b - s_a}{l} x + s_a \tag{29}$$

Or,

$$dx = \frac{l}{\Delta s} ds_x \tag{30}$$

Substituting the above Eq into (28) gives

$$\frac{dp_x}{ds_x} + \frac{p_x - K}{s_x} \mp \frac{(f - f_i) \cdot l}{\Delta s} \times \frac{p_x}{s_x} = 0 \tag{31}$$

Integrating the above equation gives

$$p_x = C \cdot \left(\frac{1}{s_x}\right)^{1 \mp \frac{(f-f_i)\cdot l}{\Delta s}} + \frac{K}{1 \mp \frac{(f-f_i)\cdot l}{\Delta s}} \tag{32}$$

In the forward slide zone, when $s_x = s_a$, then $p_x = (1\text{-}\sigma_{xa}/K)\cdot K$. The parameter σ_{xa} in the above equation consists of two parts:

$$\sigma_{xa} = \sigma_f + \sigma_{xai} \tag{33}$$

where σ_f is the forward tension, MPa, σ_{xai} is the stress of the steel tube in the x direction deduced from the core material at the outlet side, MPa, and σ_{xa} is the stress of the steel tube in the x direction at the outlet side, MPa.

$$2s_a \cdot (\sigma_f + \sigma_{xai}) - h_a \cdot \sigma_{ixa} = 2s_a \cdot \sigma_f \tag{34}$$

Then,

$$\sigma_{xai} = \frac{h_a}{2s_a} \cdot \sigma_{ixa} \tag{35}$$

Letting $\xi_1 = 1\text{-}\sigma_{xa}/K$ and $\delta_1 = (f\text{-}f_i)\cdot l/\Delta s\text{-}1$ and substituting these two equations into (32) gives:

$$p_x = \frac{K}{\delta_1} \times \left[(\xi_1\delta_1 + 1) \cdot \left(\frac{s_x}{s_a}\right)^{\delta_1} - 1\right] \tag{36}$$

In the backward slide zone, when $s_x = s_b$, then $p_x = (1\text{-}\sigma_{xb}/K)\cdot K$. The parameter σ_{xb} in the above equation consists of two parts:

$$\sigma_{xb} = \sigma_b + \sigma_{xbi} \tag{37}$$

where σ_b is the backward tension, σ_{xbi} is the stress of the steel tube in the x direction deduced by the core material at the inlet side, MPa, and σ_{xb} is the stress of the steel tube in the x direction at the inlet side, MPa.

The total equilibrium of the outer end at the inlet side can be denoted as follows:

$$2s_b \cdot (\sigma_b + \sigma_{xbi}) - h_b \cdot \sigma_{ixb} = 2s_b \cdot \sigma_b \tag{38}$$

Then,

$$\sigma_{xbi} = \frac{h_b}{2s_b} \cdot \sigma_{ixb} \tag{39}$$

Letting $\xi_2 = 1\text{-}\sigma_{xb}/K$ and $\delta_2 = (f\text{-}f_i)\cdot l/\Delta s\text{+}1$, and substituting them into Eq (32) gives

$$p_x = \frac{K}{\delta_2} \times \left[(\xi_2\delta_2 - 1) \cdot \left(\frac{s_b}{s_x}\right)^{\delta_2} + 1\right] \tag{40}$$

Considering that the bite angle is small, the wall thickness and the thickness of the core material can be assumed to be linearly distributed along the length direction of the

deformation zone, which can be denoted as follows:

$$\begin{cases} s_\gamma = \dfrac{\Delta s}{l} x_\gamma + s_a \\ h_\gamma = \dfrac{\Delta h}{l} x_\gamma + h_a \end{cases} \tag{41}$$

Then,

$$s_\gamma = \frac{\Delta s}{\Delta h} h_\gamma + s_a - \frac{\Delta s}{\Delta h} h_a \tag{42}$$

where s_γ is the wall thickness at the neutral plan, mm.

By integrating the parameter p_x among the whole deformation zone, the roll force P can be obtained as follows:

$$P = \frac{(B_{cb} + B_{ca}) \cdot K}{2} \left\{ \frac{1}{\delta_1} \int_0^{x_\gamma} \left[(\xi_1 \delta_1 + 1) \left(\frac{s_x}{s_a} \right)^{\delta_1} - 1 \right] dx + \frac{1}{\delta_2} \int_{x_\gamma}^{1} \left[(\xi_2 \delta_2 - 1) \left(\frac{s_b}{s_x} \right)^{\delta_2} + 1 \right] dx \right\} \tag{43}$$

Substituting Eq (30) into the above equation gives

$$P = \frac{(B_{cb} + B_{ca}) \cdot K}{2} \times \frac{l}{\Delta s} \left\{ \frac{(\xi_1 \delta_1 + 1) \cdot s_\gamma}{\delta_1 (\delta_1 + 1)} \left(\frac{s_\gamma}{s_a} \right)^{\delta_1} + \frac{(\xi_2 \delta_2 - 1) \cdot s_\gamma}{\delta_2 (\delta_2 - 1)} \left(\frac{s_b}{s_\gamma} \right)^{\delta_2} + \frac{1 - \xi_1}{\delta_1 + 1} \cdot s_a + \frac{1 - \xi_2}{\delta_2 - 1} \cdot s_b - \left(\frac{1}{\delta_1} + \frac{1}{\delta_2} \right) \cdot s_\gamma \right\} \tag{44}$$

where P is the roll force, N.

Then, the average unit pressure $\bar{p}$ can be deduced as follows:

$$\bar{p} = \frac{K}{\Delta s} \left\{ \frac{(\xi_1 \delta_1 + 1) \cdot s_\gamma}{\delta_1 (\delta_1 + 1)} \left(\frac{s_\gamma}{s_a} \right)^{\delta_1} + \frac{(\xi_2 \delta_2 - 1) \cdot s_\gamma}{\delta_2 (\delta_2 - 1)} \left(\frac{s_b}{s_\gamma} \right)^{\delta_2} + \frac{1 - \xi_1}{\delta_1 + 1} \cdot s_a + \frac{1 - \xi_2}{\delta_2 - 1} \cdot s_b - \left(\frac{1}{\delta_1} + \frac{1}{\delta_2} \right) \cdot s_\gamma \right\} \tag{45}$$

where $\bar{p}$ is the average unit pressure, MPa.

2.5 Solving for wall thickness

During the flat rolling process of the CORFT, considering the equilibrium for the whole deformation zone in the y direction, the roll force P should be equal to the compressive force P_i of the core material, or $\bar{p}$ should be equal to $\bar{p}_i$. The thickness s_a of the outer steel tube in the equations for the parameters $\bar{p}$ and $\bar{p}_i$ are both unknown quantities and must be solved. The solution of s_a can refer to the method for solving for the roll gap using the elastoplastic curve of the mill (P-H diagram).

As shown in Fig 5, $\bar{p}$ and $\bar{p}_i$ are both related to the wall thickness s; $\bar{p}$ increases with decreasing s, and $\bar{p}_i$ decreases with s. There are three kinds of relationships between the curves $\bar{p}$ and $\bar{p}_i$ in the range of 0~s_b: (a) Nonintersecting, (b) intersecting and the abscissa of the intersection point is s_b, and (c) intersecting and the abscissa s_C of the intersection point is less than s_b.

When the total reduction rate e_t (the reduction rate between the rolled workpiece and the preformed billet) is small, $\bar{p}_i$ can be denoted by curve a in Fig 5. In this case, the holding force on the inner surface of the steel tube provided by the core material is small because of the low core density and the wall thickness s of the outer steel tube changes little; thus, s_a equals s_b. When e_t is large, $\bar{p}_i$ can be denoted by curve c in Fig 5. In this case, the holding force on the

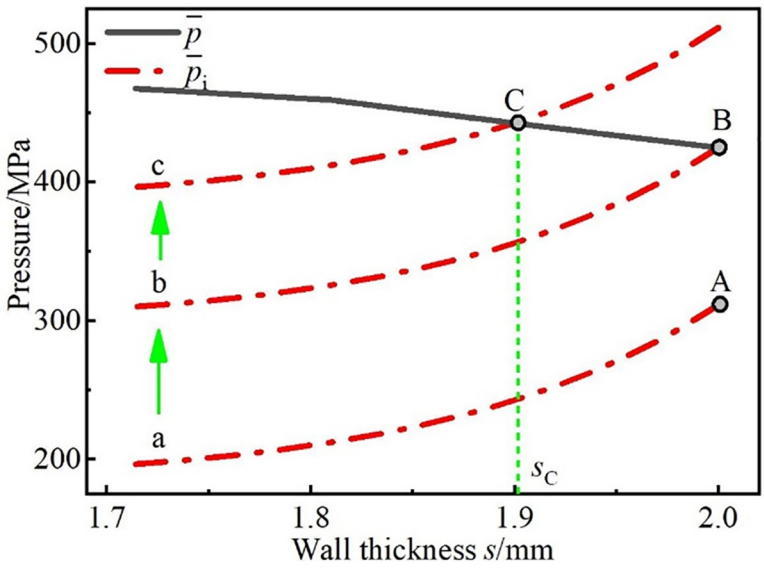

Fig 5. Solving for the wall thickness.

https://doi.org/10.1371/journal.pone.0237039.g005

inner surface of the steel tube provided by the core material is sufficient because of the large core density, and the wall thickness s of the outer steel tube decreases, Meanwhile, after the flat rolling process of the CORFT, the wall thickness s_a equals the abscissa s_C of the intersection point, or $s_a = s_C$. Thus, despite of the value of the total reduction rate e_t, Fig 5 can be used to solve for the thickness s_a.

3 Rolling experiments

3.1 Experimental procedure

Six steel tubes with dimensions of 300 mm in length, 36 mm in diameter, and 2 mm in thickness were prepared. Two tag lines (used to measure the elongation coefficient) perpendicular to the axis of each steel tube were marked to divide the steel tube into three equal parts, and the distance between the two tag lines was the initial scale length l_{s0}. The initial outer diameters D_0, initial wall thicknesses s_0, initial total lengths l_{t0}, and initial scale lengths l_{s0} of the steel tubes were measured. The BFS was dried in a muffle furnace at 300 degrees centigrade for 12 hours. Three portions of the dried BFS were measured to pack the three prepared steel tubes, and then three CORFT billets were obtained. The initial packing density of the billets were 0.97±0.001 g/cm^3.

When preparing CORFTs, first the oil stains on the inner and outer surfaces of the steel tubes were removed using anhydrous alcohol. Second, one end of each steel tube was flattened. After that, the prepared BFS was packed into the steel tubes, and the other side of each steel tube was flattened. Then, preformed billets (approximately 14 mm thick) were produced, and two parallel tag lines (used to measure the slide spread rate) were marked in the width direction of each preformed billet (the distance between the two tag lines was b_{w0}). Finally, multiple passes of flat rolling were conducted, and the CORFT products 8 mm in thickness were obtained, as shown in Fig 6. Removing the packing process, the above flow can be used to prepare tubes.

The rolling mill was a 180×260 mm drag over mill. The rolling speed was adopted as 50 mm/s, and neither lubricants nor tensions were applied to the rolling process. The

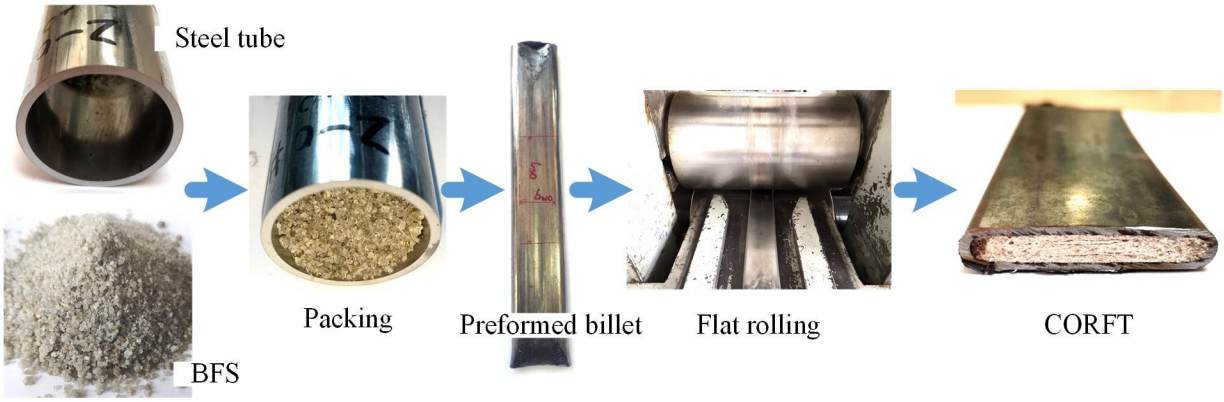

Fig 6. Experimental procedure of the CORFT.

https://doi.org/10.1371/journal.pone.0237039.g006

CORFT and the tube flat rolling experiments were repeated three times to obtain adequate accuracy.

3.2 Calculation of relevant parameters

During the flat rolling process of the CORFT, to obtain the relative density of the core material by using the experimental data, several hypotheses should be made, including:

(1) The wall thickness of the outer steel tube is uniform.

The bending segment elongates equally with the elongation of the line segment, because the outer steel tube is a continuum. The thickness of the bending segment decreases with elongation. Thus, the thickness of the bending segment is assumed to equal the thickness of the line segment, that is, the thickness of the outer steel tube is homogeneous and denoted as s_i.

(2) The slide spread of the CORFR during the flat rolling process can be neglected.

During the flat rolling process of the CORFT, the total spread of the CORFT contains the slide spread, overturn spread and drum-shaped spread. When the total reduction rate (the reduction rate for the rolled billet compare with the preformed billet) is small, only the outer steel tube of the CORFT bends; thus, the slide spread of the outer steel can be neglected. When the total reduction rate is large, the parameter B/l (the ratio of total width B of the rolled billet and the length l of the contact ace) is large, the slide spread of the outer steel can also be neglected. Thus, during the flat rolling process of the CORFT, the slide spread can be neglected despite of the value of the total reduction rate.

(3) The length of the neutral line for the outer steel tube remained unchanged during the flat rolling process.

During the flat rolling process of the CORFT, the neutral line length l_{neu} (as shown in Fig 2 (A)) of the cross section for the outer steel tube of the CORFT is not influenced by overturn spread and drum-shaped spread, and l_{neu} linearly increases as the slide spread increased. Thus, neglecting the slide spread, the l_{neu} can be assumed to remain unchanged during the flat rolling process of the CORFT.

The above hypotheses will be verified in section 4.2

The relative density z of the core material is the ratio of the density ρ and the granular density ρ_g of the core material, $z = \rho/\rho_g$. The parameter z reveals the compaction rate of the core material, and determines the performance of bending resistance, flattening resistance and corrosion resisting for the CORFT.

During each flat rolling pass, the distances between the tag lines (l_{si} and b_{wi}) are measured in the length and width directions. Then, the elongation coefficient and slide spread rate after the i-th pass can be denoted as:

$$\begin{cases} \lambda_i = \dfrac{l_{si}}{l_{si-1}} \\ \eta_i = \dfrac{b_{\mathrm{wi}} - b_{\mathrm{w0}}}{\mathrm{b_{w0}}} \times 100\% \end{cases} \tag{46}$$

where λ_i and η_{i} are the elongation coefficient and slide spread rate of the i-th pass, l_{si-1} and l_{si} are the scale lengths in the length direction before and after the i-th pass, mm, while b_{wi} and b_{w0} are the scale lengths in the width direction after the i-th pass and for the preformed billet, mm.

Considering the mass conservation of the outer steel tube, the following equation can be obtained:

$$\rho_{\mathrm{s}} \cdot s_0 \cdot b_{\mathrm{w0}} \cdot l_{\mathrm{s0}} = \rho_{\mathrm{s}} \cdot s_i \cdot b_{\mathrm{w0}} \cdot l_{\mathrm{s0}} \cdot \prod_{j=1}^{i} \lambda_i \tag{47}$$

where $\prod_{j=1}^{i} \lambda_i = \lambda_1 \times \lambda_2 \times \cdots \times \lambda_i$, ρ_{s} is the density of the steel tube, g/cm^3, l_{s0} and b_{w0} are the distances between the parallel flag lines, respectively, in the length and width directions, mm, s_0 is the initial thickness of the steel tube, mm, l_0 is the initial length of the steel tube, mm, and s_i is the wall thickness after the i-th pass.

Then, s_i can be deduced as follows:

$$s_i = \frac{s_0}{\prod_{j=1}^{i} \lambda_i} \tag{48}$$

During the flat rolling process of the CORFT, the length of neutral line can be assumed to remain unchanged. Then,

$$\pi \cdot (D_0 - s_0) = \pi \cdot (H_{\mathrm{a}i} - s_i) + 2B_{ci} \tag{49}$$

where $H_{\mathrm{a}i}$ is the thickness of the rolled billet after the i-th pass, and B_{ci} is the contact width between the rolled billet and the roll after the i-th pass.

B_{ci} can be deduced from the above equation as shown:

$$B_{ci} = \frac{\pi \cdot (D_0 - H_{\mathrm{a}i} - s_0 + s_i)}{2} \tag{50}$$

The section areas for the core material of the rolled billet before and after deformation (F_0 and F_i) can be obtained as follows:

$$\begin{cases} F_0 = \dfrac{\pi}{4} \cdot (D_0 - 2s_0)^2 \\ F_i = \dfrac{\pi}{4} \cdot (H_{\mathrm{a}i} - 2s_i)^2 + B_{ci} \cdot (H_{\mathrm{a}i} - 2s_i) \end{cases} \tag{51}$$

where F_0 and F_i are the section areas for the core material of the preformed billet and the rolled billet after the i-th pass, mm^2.

Considering the mass conservation of the core material, it can be deduced that:

$$z_0 \cdot \rho_{\mathrm{g}} \cdot F_0 = z_i \cdot \rho_{\mathrm{g}} \cdot F_i \cdot \prod_{j=1}^{i} \lambda_i \tag{52}$$

where z_0 and z_i are the initial relative density and the relative density after the i-th pass of the core material, and ρ_g is the density of the BFS particles, g/cm^3.

By substituting Eq (51) into (52), z_i can be obtained:

$$z_i = \frac{\frac{\pi}{4} \cdot (D_0 - 2s_0)^2}{\left[\frac{\pi}{4} \cdot (H_{ai} - 2s_i)^2 + B_{ci} \cdot (H_{ai} - 2s_i)\right] \cdot \prod_{j=1}^{i} \lambda_i} \times z_0 \tag{53}$$

4 Results and discussion

4.1 Comparison of the CORFT and the tube experimental results

Multiple passes of flat rolling experiments on the CORFTs and the tubes were conducted, and the products of the CORFT and the tube were obtained and are shown in Fig 7(A). Sections of the rolled billets were cut out with total thicknesses (H) of approximately 36, 12, 11, 10 and 9 mm. The scan images of the sections of the CORFTs and the tubes are shown in Fig 7(B). As shown in Fig 7(B), the wall thickness of the CORFTs decreased and the wall thickness of the tubes remained unchanged with the decrease in H. For the CORFTs, the normal pressure p_{ix} on the inner surfaces of the steel tubes provided by the core material became sufficient to promote the thinning of the steel tubes when H decreased to a certain value. In this case, the wall thickness decreased with the increase of the flat rolling passes. For the tubes, the normal pressure on the inner surfaces of the steel tubes equaled zero because the inner surfaces of the steel tubes were free surfaces. Thus, the outer steel tubes bent only with the increase of the flat rolling passes, and the wall thickness remained unchanged.

The original data of the workpieces after the flat rolling process of the CORFT are shown in Table 1. The table includes thickness H_i, total width B_i, and the distances between the flag lines in the length direction l_{si} and the width direction b_{wi}.

To study the deformation laws for multiple passes in the flat rolling process of the CORFT and the tube, trend charts between the relative density z of the core material and the total reduction rate e_t were drawn, as shown in Fig 8(A). Trend charts between the ratio of thinning τ and the total width B of the rolled billets and the e_t were drawn, as shown in Fig 8(B) and 8(C).

As shown in Fig 8(A), with the increase in e_t, the relative density z of the core material increased and then remained unchanged. When e_t was less than or equaled to e_c, the s

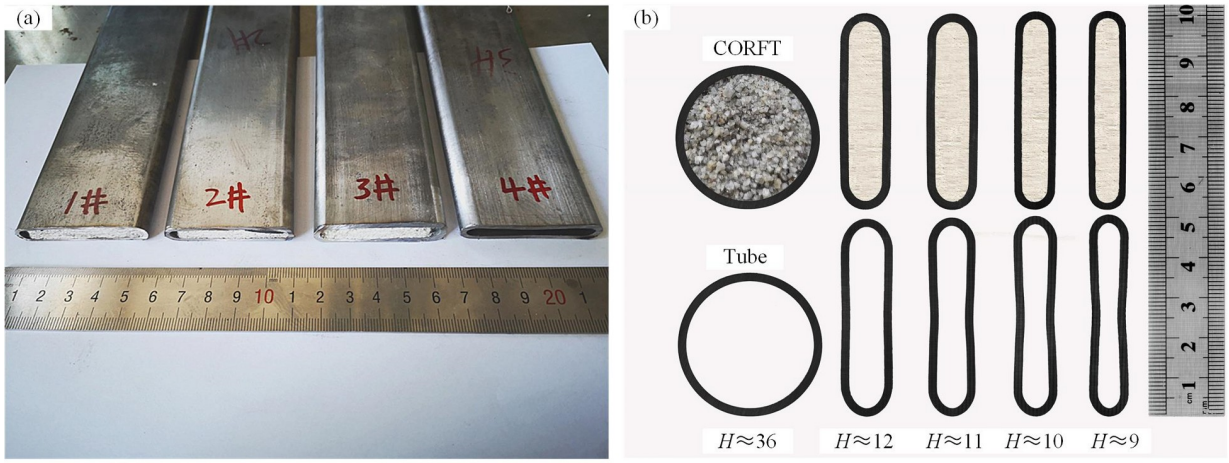

Fig 7. Pictures of the CORFTs and the tube. (a) Products, and (b) scanning image of the section.

https://doi.org/10.1371/journal.pone.0237039.g007

Table 1. Original data of the flat rolling experiments of the CORFT (mm).

Thickness H_i	Total width B_i	Distance between flag lines in length direction l_{si}	Distance between flag lines in width direction b_{wi}
14.01	47.60	100.04	31.15
12.04	48.74	101.79	30.98
11.03	49.14	106.580	31.30
9.98	49.53	116.630	31.60
8.96	49.90	128.750	31.91

https://doi.org/10.1371/journal.pone.0237039.t001

remained unchanged. Thus, with the increase in e_t, the inner area of the steel tube of the CORFT decreased. Then z and p_{ix} increased. the Trend for the ratio of thinning and elongation increased and then the growth rate of z decreased until it approached zero. When the growth rate of z was zero and e_t increased, the z remained unchanged, that is, z had an ultimate value of z_U, which was 0.868.

As shown in Fig 8(B), with increasing e_t, the ratio of thinning τ for the tube was always zero. The value of τ for the CORFT was zero at first, and when e_t became larger than e_c, τ started to increase, and the growth speed increased first and then remained unchanged. For the flat rolling process of the tube, only the outer steel tube bent, and the wall thickness remained unchanged because the inner surface of the steel tube was a free surface. For the flat rolling process of the CORFT at the initial stage of deformation, p_{ix} increased with increasing e_t, but p_{ix} was not sufficient to facilitate the thinning of the outer steel tube; thus, the value of τ was always approximately zero. When e_t became larger than e_c, p_{ix} became sufficient, and τ began to increase. Meanwhile, the growth speed of τ increased first and then remained unchanged because z increased first and then remained unchanged; that is, p_{ix} followed the same change law.

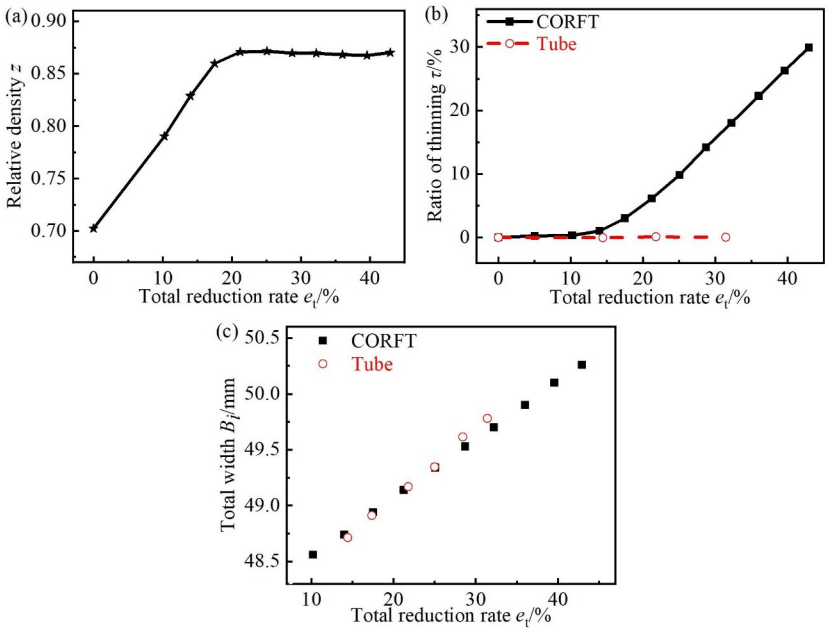

Fig 8. Parameters deduced by the flat rolling experiments. (a) Relative density of the CORFT, (b) ratio of thinning for the CORFT and the tube, and (c) total width of the CORFT and the tube.

https://doi.org/10.1371/journal.pone.0237039.g008

As shown in Fig 8(C), the total width B of the CORFT and tube both increased with increasing e_t, and their curves were basically in coincidence. For the flat rolling process of the CORFT and tube, with increasing e_t, B increased because fresh metal turns over to the roll surface continuously.

4.2 Verification of several hypotheses

The line segment thickness (the assumed thickness adopted in the uniform thickness hypothesis) s, the length of neutral line l_{neu} and section area F_{sec} for different rolling process of the CORFT (shown in Fig 7(B)) were measured. Then, the average thickness $\bar{s}$ was calculated as follows;

$$\bar{s} = \frac{F_{sec}}{l_{neu}} \tag{54}$$

The trend diagrams of the thickness, the length of the neutral line and the slide spread rate in the different total reduction rate e_t are given in Fig 9. As shown in Fig 9(A), with the increase in the reduction rate e_t, the length of the neutral line l_{neu} changed little; the change rate was within the range of -2.65% to 0%. Fig 9(A) verified the feasibility of the hypothesis regarding neglecting the change in l_{neu} during the rolling process of the CORFT. As shown in Fig 9(B), with the increase in the total reduction rate e_t, the difference between the assumed thickness s and the average thickness $\bar{s}$ was very small, the error rate was within the range of -1.66% to 0%.

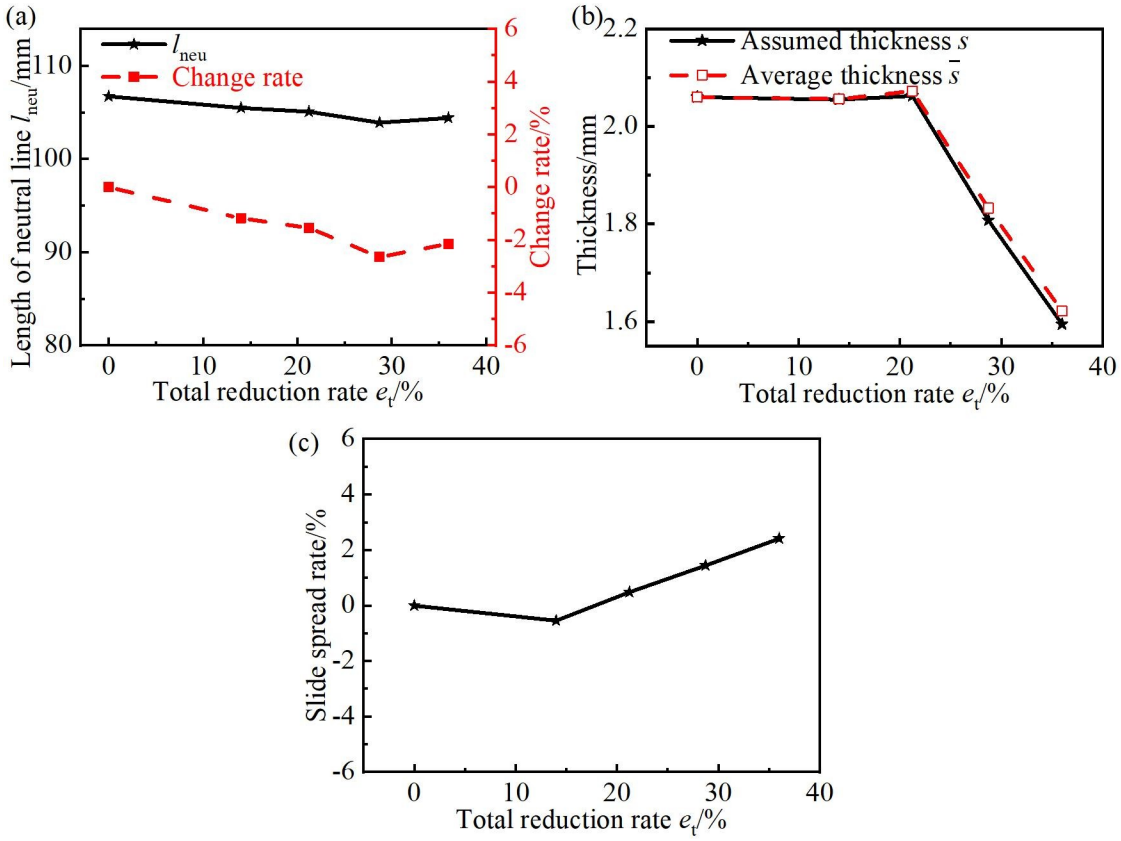

Fig 9. Validation of hypotheses on thickness, neutral line and slide spread rate. (a) Length of the neutral line, (b) comparison of the assumed thickness and average thickness, and (c) slide spread rate.

https://doi.org/10.1371/journal.pone.0237039.g009

Fig 9(B) verified the feasibility of the uniform thickness hypothesis (the thickness of the line segment was equal to the bending segment). As shown in Fig 9(C), with the increase in the total reduction rate e_t, the slide spread rate was always very small; the value was within the range of -0.5% to 2.4%. Fig 9(C) verified the feasibility of the hypothesis regarding neglecting the slide spread rate during the rolling process of the CORFT.

4.3 Precision analysis of theoretical models

For the flat rolling process of the CORFT, the charts for the curves between τ and e_t are shown in Fig 10(A). The above two charts show that, with increasing e_t, both the theoretical and the experimental values of τ were approximately zero at first. When e_t became larger than e_c, τ began to increase, and the growth speed increased first and then remained unchanged. The error value between the two τ values was within the range of -0.27% to 1.14%. For the flat rolling process of the CORFTs, the charts for curves between the z and the e_t are shown in Fig 10 (B). The above two charts show that, with increasing e_t, both the theoretical and the experimental values of z increased first and then remained unchanged. The error ratio between the two z values was within the range of -1.05% to 0.99%. In addition, the theoretical and the experimental z_U values were 0.876 and 0.868, respectively. The error ratio between the two z_U values was within 1.0%. Fig 10 validated the accuracy of predicting τ, z and z_U using the theoretical equations.

4.4 Effect of rolling parameters on roll force

During the rolling process of CORFTs, the roll force was an important parameter. It was related to the selection of rolling mills and the energy consumption. The curves between the roll force and total reduction rate e_t are drawn in Fig 11. The curves demonstrate that the roll force increased with increasing e_t, and the increasing speed decreased first and then stabilized at a small value.

Fig 11(A) shows that the roll force increased with the increasing initial wall thickness s_0. With the increase in the parameter s_0, the area ratio φ between the core material and the steel tube in a section decreased and the thickness reduction of the outer steel tube increased. Thus, the roll force increased with increasing s_0.

Fig 11(B) shows that at the same mass ratio Φ, the roll force increased with increasing z_0 when the e_t was small, and remained unchanged with the change of z_0 when e_t was large. When e_t was small, the volumetric shrinkage of the core material was large, and the reduction

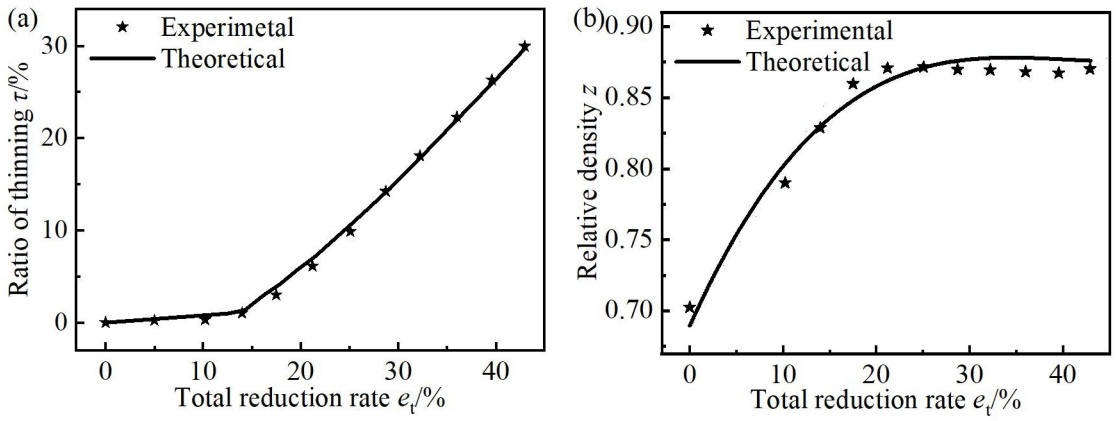

Fig 10. Comparison of the analytical and experimental results of the CORFT. (a) Ratio of thinning, and (b) relative density.

https://doi.org/10.1371/journal.pone.0237039.g010

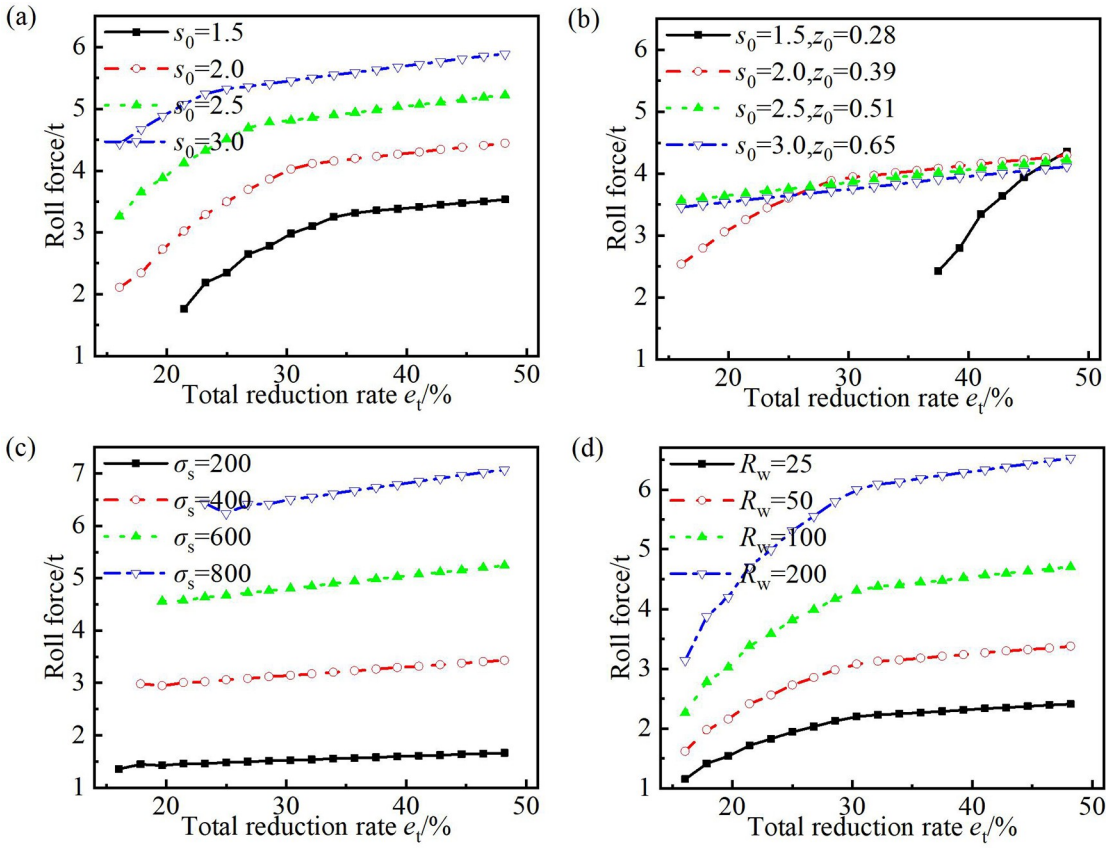

Fig 11. Effect of parameters on roll force. (a) Filling wall thickness, (b) filling wall thickness with the same mass ratio between the core material and the steel tube in a section, (c) yield strength of the steel tube, and (d) work roll radius.

https://doi.org/10.1371/journal.pone.0237039.g011

of wall thickness for the outer steel tube increased with increasing z_0; thus, the roll force increased. When e_t was large, the volumetric shrinkage was small, the relative density of the core material approached one value (z_U), and the area ratio φ remained unchanged with increasing z_0; thus, the roll force remained unchanged.

Fig 11(C) shows that the roll force increased with increasing σ_s of the steel tube. With the increase in σ_s, the deformation resistance increased and then the roll force increased.

Fig 11(D) shows that the roll force increased with increasing work roll radius R_w. With increasing R_w, the length of the deformation zone increased and then the roll force increased.

The maximum roll force is useful in mill design, and it needs to be quantitative analyzed, as shown in Fig 12. The above graph shows that the parameters s_0, σ_s and R_w had obvious influences on the maximum roll force, but s_0 had little influence on the maximum roll force when Φ remained unchanged. When z_0 remained unchanged and s_0 increased from 1.5 mm to 3.0 mm, the value of the maximum roll force increased from 3.53 t to 5.89 t with a changing rate of 66.9%. When Φ remained unchanged and s_0 increased from 1.5 mm to 3.0 mm, the value of the maximum roll force was within the range of 4.11 t to 4.36 t. When σ_s increased from 200 MPa to 800 MPa, the value of the maximum roll force increased from 1.67 t to 7.07 t with a changing rate of 323.4%. When R_w increased from 25 mm to 200 mm, the value of the maximum roll force increased from 2.41 t to 6.53 t with a changing rate of 170.1%.

Overall, the limiting conditions for larger maximum roll force included a larger initial wall thickness, a higher yield strength of the steel tube, and a larger work roll radius.

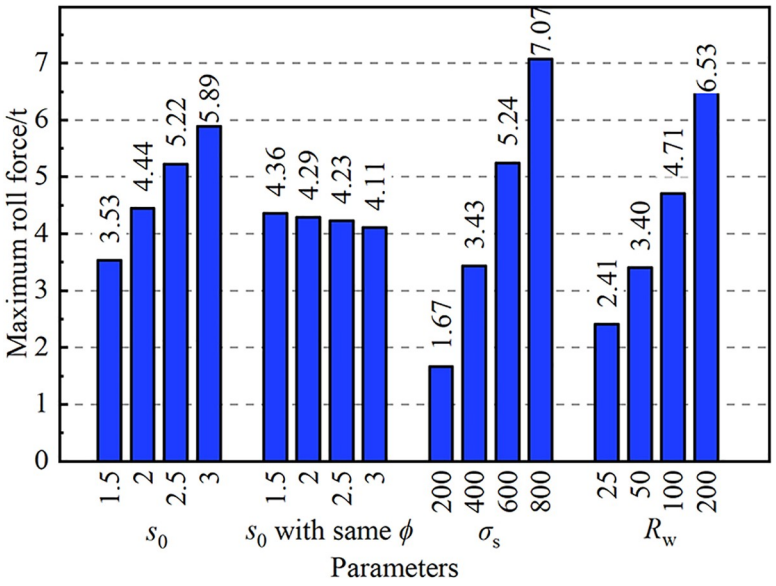

Fig 12. Effect of parameters on maximum roll force.

https://doi.org/10.1371/journal.pone.0237039.g012

4.5 Effect of rolling parameters on the ultimate value of the relative density

z_U is an important parameter; with a larger z_U, the holding force on the inner surface of the steel tube provided by the core material was larger, and the performance of flattening resistance for the CORFT was better. To study the influence of different rolling parameters on z_U, a quantitative study on z_U was conducted, and the results are shown in Fig 13.

Fig 13 shows that the parameters s_0, z_0 and σ_s had obvious influences on z_U, but s_0 had little influence on z_U when Φ remained unchanged. When z_0 remained unchanged and s_0 increased from 1.5 mm to 3.0 mm, the value of z_U increased from 0.861 to 0.890 with a changing rate of

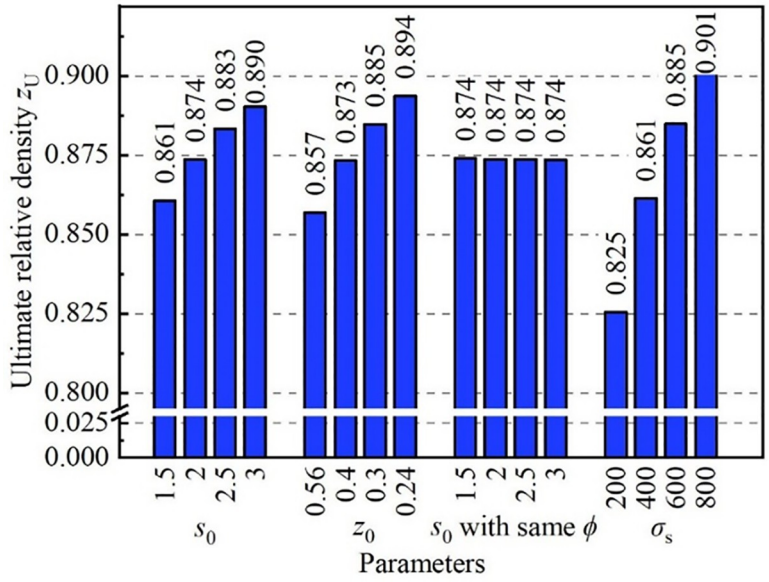

Fig 13. Effect of parameters on the ultimate value of the relative density.

https://doi.org/10.1371/journal.pone.0237039.g013

3.4%. When s_0 remained unchanged and z_0 decreased from 0.56 to 0.24, the value of z_U increased from 0.857 to 0.894 with a changing rate of 4.3%. When Φ remained unchanged and s_0 increased from 1.5 mm to 3.0 mm, the value of z_U always equaled 0.874. When σ_s increased from 200 MPa to 800 MPa, the value of z_U increased from 0.825 to 0.901with a changing rate of 9.2%.

Overall, in order to obtain a CORFT with good flattening resistance performance, that is a CORFT with a high z_U, rolling parameters with a small Φ and a large σ_s were adopted. In order to obtain a small Φ, rolling parameters with a large s_0 or a small z_0 were adopted.

5 Conclusions

(1) Adopting the plan deformation condition, an analytical model based on the slab method was developed. This model contained equations to calculate wall thickness s, relative density z of the core material, and roll force P.

(2) Validation experiments of flat rolling were conducted, and workpieces of the CORFT were obtained. Parameters including the ratio of thinning and relative density were calculated and compared with the theoretical values. The error value relative to the experimental data was -0.27% to +1.14% for the ratio of thinning τ and was -1.05% to +0.99% for the relative density z. The accuracy of the equations can satisfy the precision requirements in engineering.

(3) The influences of rolling parameters on roll force were studied. The limiting condition for larger maximum roll force included: larger initial wall thickness, higher yield strength of the steel tube, and larger work roll radius. When s_0 increased from 1.5 mm to 3.0 mm, σ_s increased from 200 MPa to 800 MPa, or work roll radius increased from 25 mm to 200 mm, the maximum roll force increased from 3.53 t to 5.89 t, from 1.67 t to 7.07 t, or from 2.41 t to 6.53 t, respectively.

(4) To improve the performance of bending resistance, flattening resistance and corrosion resistance for the CORFT, the influences of rolling parameters on z_U were studied, and the process with a larger σ_s, smaller z_0, and larger s_0 was adopted.

Author Contributions

Conceptualization: Junlong Qi.

Data curation: Xiangkun Sun.

Formal analysis: Junlong Qi.

Validation: Haitao Gao.

Writing – original draft: Junlong Qi.

Writing – review & editing: Junlong Qi, Xianghua Liu.

References

1. He K, Wang L. A review of energy use and energy-efficient technologies for the iron and steel industry. Renewable and Sustainable Energy Reviews. 2017; 70: 1022–1039. https://doi.org/10.1016/j.rser.2016.12.007
2. Liu XH, Gao HT, Zhang SL, Qi JL. A kind of Core Filled Tube and it's preparation method. CN; 2017-05-31.
3. Liu XH, Gao HT, Peng LG, Dong XX. A kind of Core Filled Tube/Core Filled Steel Bar and it's preparation method. CN; 2014-08-27.
4. Hideo H, Akiyasu Y, Hidenori H, Ma YW. Recent advances in iron-based superconductors toward applications. Materials Today. 2018; 21: 278–302. https://doi.org/10.1016/j.mattod.2017.09.006

5. Liu Y, Wang X, Gao Y. Three-dimensional multifilament finite element models of Bi-2212 high-temperature superconducting round wire under axial load. Composite Structures. 2019; 211: 273–286. https://doi.org/10.1016/j.compstruct.2018.12.027
6. Zhang S, Li C, Ma X, Feng J, Shao B, Liu X, et al. Fabrication of Bi-2223 High Temperature Superconducting Tapes With Groove Rolling Process. Ieee Transactions on Applied Superconductivity. 2020; 30: 1–4. https://doi.org/10.1109/TASC.2020.2978784
7. Huang H, Ma Y, Yao C, Zhu Y, Zhang X, Dong C, et al. Influences of Tape Thickness on the Properties of Ag-Sheathed Sr 1-x K x Fe 2 As 2 Superconducting Tapes. Ieee Transactions on Applied Superconductivity. 2018; 28: 1–5. https://doi.org/10.1109/TASC.2017.2779751
8. Liang X, Liu Y, Li H, Gan Z, Liu B, He Y. An investigation on microstructural and mechanical properties of powder metallurgical TiAl alloy during hot pack-rolling. Materials Science and Engineering: A. 2014; 619: 265–273. https://doi.org/10.1016/j.msea.2014.09.091
9. Nagasekhar AV, Tick-Hon Y, Ramakanth KS. Mechanics of single pass equal channel angular extrusion of powder in tubes. Applied Physics A. 2006; 85: 185–194. https://doi.org/10.1007/s00339-006-3677-y
10. Han Z, SkovHansen P, Freltoft T. The mechanical deformation of superconducting BiSrCaCuO/Ag composites. Superconductor Science & Technology. 1997; 10: 371–387. https://doi.org/10.1088/0953-2048/10/6/001
11. Korzekwa DA, Bingert JF, Podtburg EJ, Miles P. Deformation processing of wires and tapes using the oxide-powder-in-tube method. Applied Superconductivity. 1994; 2: 261–270. https://doi.org/10.1016/0964-1807(94)90012-4
12. Pandheeradi M, Vaze SP, Yuan DW, Kuhn HA. Modeling and experimental validation of superconductor tape rolling. Journal of Manufacturing Science and Engineering, Transactions of the ASME. 2001; 123: 665–673. https://doi.org/10.1115/1.1371929
13. Lu Y. Optimization of Cross-sectional Shapes of the Bi-2223/Ag Wires before Flat Rolling. Chinese Journal of Mechanical Engineering. 2009; 22: 890. https://doi.org/10.3901/CJME.2009.06.890
14. Lu YJ. Deformation analysis for the superconductor-silver interface in the Bi-2223/Ag tape rolling process. Proceedings of the 2017 7th International Conference on Manufacturing Science and Engineering (Icmse 2017). 2017; 128: 233–240. https://doi.org/10.2991/icmse-17.2017.42
15. Jiang ZY, Tieu AK. A 3-D finite element method analysis of cold rolling of thin strip with friction variation. Tribology International. 2004; 37: 185–191. https://doi.org/10.1016/S0301-679X(03)00049-5
16. Cavaliere MA, Goldschmit MB, Dvorkin EN. Finite element analysis of steel rolling processes. Computers & Structures. 2001; 79: 2075–2089. https://doi.org/10.1016/S0045-7949(01)00055-4
17. Qi J, Liu X, Gao H, Chen J, Hu X, Yan S. Experiment and analytical model based on slab method for drawing process of core filled tube. International Journal of Mechanical Sciences. 2020; 165: 105152. https://doi.org/10.1016/j.ijmecsci.2019.105152
18. Rowe GW. Elements of metalworking theory. 1979.
19. Razani NA, Mollaei Dariani B, Soltanpour M. Analytical approach of asymmetrical thermomechanical rolling by slab method. The International Journal of Advanced Manufacturing Technology. 2018; 94: 175–189. https://doi.org/10.1007/s00170-017-0801-4
20. Sun J, Peng Y, Dong Z, Du X. Study on asymmetrical deformation and curvature of heavy cylinder rolling. International Journal of Mechanical Sciences. 2017; 133: 720–727. https://doi.org/10.1016/j.ijmecsci.2017.09.025
21. Wang HY, Li X, Sun J, Wang ZH, Zhao DW, Zhang DH. Analysis of sandwich rolling with two different thicknesses outer layers based on slab method. International Journal of Mechanical Sciences. 2016; 106: 194–208. https://doi.org/10.1016/j.ijmecsci.2015.12.021